

EXPERIMENTAL STUDY OF PRESSURE DROP AND MODELING OF INTERFACIAL SHEAR FOR VERTICAL ANNULAR FLOW

Liang-ming Pan*, Hui He, Yao Wu

Chongqing University

Department of Nuclear Engineering, Chongqing University, Chongqing 400044, P.R. China
cneng@cqu.edu.cn; 784381263@qq.com; dlwuyao@cqu.edu.cn

Peng Ju, Takashi Hibiki, Mamoru Ishii

School of Nuclear Engineering

Purdue University

400 Central Dr., West Lafayette, IN 47907-2017, USA
pju@purdue.edu; hibiki@ecn.purdue.edu; ishii@purdue.edu

ABSTRACT

The knowledge of the interfacial shear stress is not only essential for estimating the pressure drop but also is fundamental for modelling two-phase flow phenomena. Most annular flow interfacial shear stress models in the open literature are formulated based upon the sand-roughness model, which diverge from reality to some extent because of the mobility of gas-liquid interface. In view of this, a prediction model of gas-liquid interfacial shear stress for vertical annular flow has been proposed, which takes the interfacial characteristics into account, i.e. the local disturbance wave shapes obtained through processing the time trace of liquid film thickness that is measured using high-speed videos and extracted by the Matlab code in our previous work. What is more, the influence of the entrainment-deposition process and formation of gas eddy caused by the disturbance wave height when the gas core moves through the disturbance wave and subsequently encounters an abrupt expansion on the interfacial shear stress are incorporated into the model. The results predicted by the current model show that the interfacial shear stress has an increasing trend for the increase of both gas and liquid superficial velocities, and the non-dimensional pressure drop originating from the interfacial shear stress is in the form of $c_{fs} = 33.6 \text{Re}_g^{-0.91} \text{Re}_f^{0.30}$.

KEYWORDS

Annular Flow, Interfacial Shear Stress, Disturbance Wave Height, Pressure Drop

1. INTRODUCTION

Gas-liquid annular flow is one of the most common two-phase flow patterns that arise in practice. It is normally characterized by a gas core flowing through the center of the tube; a part of the liquid, as a thin liquid film, flowing on the tube wall. The thin liquid film is composed of both thin, slow-moving base film and thick, fast-moving disturbance wave [1, 2]. Annular flow is also typical of high interfacial shear stress, caused by high shear velocities introduced by the high gas rates, the continuous processes of droplet entrainment into the gas core and droplet deposition out of the gas core, and the characteristics of the disturbance waves include the interface structure, i.e. the wave height, spacing, velocity, etc. The interfacial shear stress being treated as mainly part of pressure drop (one of the most important parameters used to characterize a flow system) has been the subject of extensive studies in the past.

The most widely used model for interfacial shear stress using a friction factor was proposed by Wallis [3] who treated the liquid film as a type of wall roughness and defined an interfacial friction factor, f_i , as

$$f_i = 0.005 \left(1 + 300 \frac{\delta}{D} \right) \quad (1)$$

It derived from an analogy to a simplified form of the friction correlation in fully rough pipes, valid over a small range of roughness. Over the years, the Wallis correlation has been modified in order to match the experimental results over a larger range of film thickness. Those modifications consisted mostly of the small changes in the form and in the constants of the Wallis correlation and the inclusion of a Reynolds number dependency. Lopes and Dukler [4] and Fore et al. [5] demonstrated that the introduction of a Reynolds number dependency could be justified by the occurrence of transition roughness, instead of full roughness. However, no physically based justification was given for this suggestion. Also, it was not clear from their work how transition roughness should be implemented correctly in the correlation.

Kumar et al. [6] summarized the deficiency in the existing models and developed a new interfacial shear stress model called the law of the interface model based on the law of the wall approach in turbulent flows. However, the prediction of the void fraction in their model was less accurate due to the lack of a good mechanistic model for entrainment. Oliemans et al. [7] presented an investigation into the reliability with which pressure loss, film thickness and liquid entrainment can be predicted by an annular flow model that was based on the well-known two-fluid (separated flow) concept and new correlations for interfacial friction and liquid fraction entrained were proposed using data compiled previously at AERE Harwell. Alves et al. [8] proposed a mechanistic two fluid model for annular flow in vertical which was similar to the approach used in development of stratified flow model enabled detailed prediction of the annular flow characteristics, including the velocity distribution, liquid fraction entrained, gas void fraction, and pressure-gradient. Because Alves's model was in possess of physical nature, it was used frequently in Alamu's thesis [9] to validate experimental results of his study. Whereas, the development of their interfacial shear stress model by mean of two-fluid concept was of little concern liquid film characteristics. Similar situation was encountered in application of the momentum balance in the axial direction of the gas core to obtain the interfacial shear stress [10, 11], although in this connection it was convenient for adding influence factors to the interfacial shear stress such as gravity, entrainment and deposition, etc. Maron et al. [12] presented a new approach towards the prediction of the interfacial friction factor in two-phase wave film flow and proved that the interfacial

shear stress and pressure drop were directly related to the waviness of the film and the mobility of the interface. They evaluated the role of interfacial mobility, differentiating between the wavy film and the solid boundary, which indicated that the interfacial shear stress was related to both the wave structure and the hydrodynamic features of the wave. They also concluded that the difficulties in predicting the interfacial shear stress evolved from the complicated wave structure of the interface and the liquid entrainment and deposition processes. Therefore, the liquid entrainment and deposition processes were considered indirectly by introducing a momentum recovery coefficient arbitrarily. Asali et al. [13] developed an equation for the entrainment which interpreted it as resulting from a balance between the rate of atomization of the wall film and the rate of deposition of droplets entrained in the gas. The results were used to develop design methods to predict the frictional pressure loss and the film height. Wang et al. [14] investigated the influences of wave height on the interfacial friction in annular gas-liquid flow and found that the friction factor in annular two-phase flow decreased less significantly with the decrease of the relative interfacial roughness than that in single-phase flow, which could be explained by the flat wave shape in annular flow.

Based on the review of the existing models and from the perspective of modeling of the interfacial shear stress for annular flow, emphasis should be put on the the gas-liquid interfacial structures and entrainment-deposition process. A fundamental understanding of the interfacial properties mainly including the interfacial roughness and some special phenomena such as entrainment and deposition is critical for better predictions of the pressure drop and interfacial shear stress in annular two-phase flow. What is more, the mobility of gas-liquid interfacial which is mainly different from the rough solid surfaces should be taken into account. However, few of the researches in the open literature are devoted to those matters mentioned above in detail. The principal objectives of this paper are to develop an interfacial shear stress model which takes the interfacial characteristics, entrainment-deposition process and gas eddy effect into account.

2. EXPERIMENTAL DETAILS

The two-phase vertical upward annular flow experiments have been performed on an air-water test facility available in TRSL (Thermal-hydraulics and Reactor Safety Laboratory) of Purdue University. Figure 1 is the schematic of test facility. The liquid flowing from the accumulator passes through a ball valve and a liquid magnetic flowmeter delivering to the buffer channel to distribute water to test section uniformly through three directions which have 120° angles to each other. Compressed air from gas storage tank passes through a ball valve, a filter and an air rotameter, then mixes with liquid in the two phase mixture injection system. The water flow rate is measured by magnetic flowmeter with an accuracy of $\pm 1\%$, and the air flow rate is set and measured by a rotameter with an accuracy of $\pm 4\%$ of full scale. Water is injected into an air-water mixture injection unit where a bubble generator is located. A sparger with an average pore size of 10 μm is employed as the bubble generator, which produces near uniform bubbles of approximately 1-2 mm in diameter at the inlet of the test section. This method can produce near uniform gas phase at the inlet of the test section, and it is helpful in generation of annular flow with minimum initial entrainment and entrance effect. The desired gas and liquid flow rate can be obtained by adjusting the ball valve and a frequency conversion pump respectively. Then the two-phase mixture enters into a transparent tubular PMMA test section with inner diameter $D=2.54$ cm. Along with the test section, three impedance void meters are located at three positions, namely, 0.637 m, 2.159 m and 3.683 m from the inlet vertically along the test section respectively. Since air-water mixture injection unit is employed at both the top and the bottom of each test section (left side with inner diameter $D=2.54$ cm, right side with inner diameter $D=5.08$ cm), so that the experimental loop is capable of operating in both upward and downward flow configurations. However, the current tests are tailored to the upward annular flow in the tubular PMMA test section having an inside diameter of 2.54 cm.

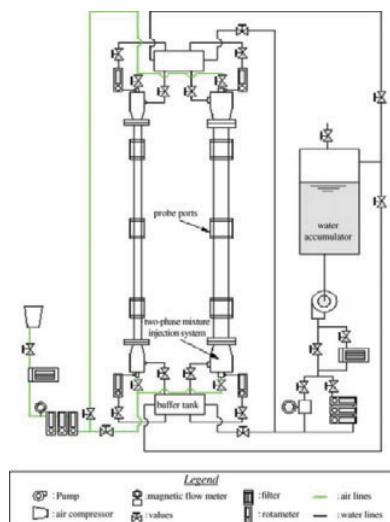


Fig. 1. Schematic of the test facility

2.1. Pressure Drop Measurement

The pressure and differential pressure measurements are conducted by a pressure gauge at the test section inlet and a differential pressure transducer at three probe ports, respectively. The accuracies of the pressure gauge and the pressure transducer are within $\pm 3\%$ of span and

within $\pm 1\%$ of full scale, respectively. To estimate test section conditions accurately, differential pressure and gauge pressure measurements are taken simultaneously. The pressure drop is evaluated by processing the upstream two differential pressure transducer signals. To avoid ambiguities in the pressure drop measurements associated with the presence of two phases in the tapping lines a liquid purge system (0.1~1% of the total liquid flow rate) is installed. The signals from the pressure gauge and differential pressure transducers are sent to a computer equipped with a data acquisition card and the sampling frequency is 10000 Hz. Experiments have been performed with five different gas phase superficial velocities, and three different liquid phase superficial velocities at ambient temperature and atmospheric pressure respectively.

Generally, the pressure drop increases with the increase of gas superficial velocity at a constant liquid superficial velocity as illustrated in Fig. 2, which are similar to others in the literature [9, 14]. Because in the annular flow region gas superficial velocity is high enough to cause high friction pressure drop, which is dominant in the total pressure drop and higher than gravitational pressure drop. In addition, with respect to the annular flow, the entrained droplets can be relatively important. The mechanism of transfer of momentum by the convection of droplets proposed by Fore et al. [10] is crucial for the pressure drop, which can equal as much as 20% of the total pressure-gradient. Based upon Ishii and Mishima [15], the entrained droplets also increase with the increase of gas and liquid superficial velocity, resulting in the higher pressure drop.

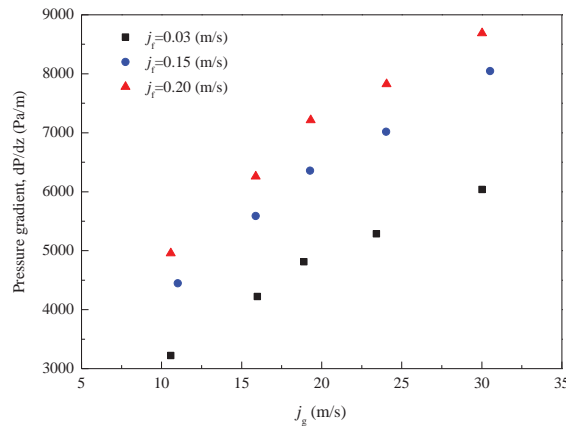


Fig. 2. Pressure gradient vs. gas superficial velocity

3. DESCRIPTION MODEL

3.1. Physical Model

When a gas phase flows over a thin liquid film, several different flow regimes are possible depending on the magnitude of the gas phase velocity. Far away from the entrance region, the interface is relatively stable with a relative small gas velocity. However, as the gas phase velocity increases, the disturbance wave will appear caused by a small interfacial perturbation which is known as Kelvin-Helmholtz instability. Being treated as a component of the thin liquid film, disturbance wave is the most dramatic phenomena in the two phase gas-liquid annular flow, because of which the disturbance wave can cause a substantial increase in mass and energy transport at the two-phase interface, also result in phenomena of entrainment, deposition and eddy. Physical observations elucidate [16] that the liquid droplets are entrained in the front region of the disturbance wave. Their research works show that droplets entrainment fraction cannot be measured until after disturbance waves appear in the annular flow. It is considered that the droplets originate from large disturbance waves in the liquid film. Subsequently, the droplets are injected into the gas core, accelerated to reasonably high velocity compared with the slow moving liquid film, and the droplets in the gas core continuously deposit on the film in a process called droplet deposition. Therefore, from the perspective of physical process of entrainment and deposition, an integrated disturbance wave can be divided into two parts, i.e. control volume one and volume two representing the front and rear of the disturbance wave respectively, as can be seen from Fig. 3. Usually, the slope of the leeward face changes more abruptly than the slope of the upwind face [17].

Given that a part of the liquid flows as entrained liquid droplets in the gas core, the density and the velocity of the gas core must be defined for the purposes of this analysis. By using a homogeneous flow assumption according to Holowach et al. [18], the density of the gas core, ρ_g^* , is defined in terms of the void fraction, α_g , and the volume fraction occupied by entrained liquid droplets, α_e .

$$\rho_g^* = \frac{\alpha_g}{\alpha_e + \alpha_g} \rho_g + \frac{\alpha_e}{\alpha_e + \alpha_g} \rho_f \quad (2)$$

Where ρ_g and ρ_f are the liquid and gas densities respectively. The principal objective of use of Eq. 2 is that α_g can be obtained directly by using the impedance void meters in the experiment. The volume fraction occupied by entrained liquid droplets, α_e , can be obtained by mean of Ishii and Mishima [15] who developed following correlation for the prediction of the entrainment fraction in quasi-equilibrium annular flow region (fully developed region).

$$E = \tanh(7.25 \times 10^{-7} We^{1.25} Re_f^{0.25}) \quad (3)$$

Where We is the Weber number being defined as,

$$We = \frac{\rho_g j_g^2 D}{\sigma} \left(\frac{\Delta \rho}{\rho_g} \right)^{1/3} \quad (4)$$

It is convenient to work on this matter in a frame moving with the velocity u_p with respect to the disturbance wave peak as shown in Fig. 3. u_p is the disturbance wave propagation velocity can be obtained from Berna et al. [19] who proposed a new wave velocity with high accuracy by summarizing and comparing many wave velocity corrections and experimental data.

$$\frac{u_p}{\sqrt{\frac{\rho_g j_g + \sqrt{\rho_f j_f}}{\sqrt{\rho_g} + \sqrt{\rho_f}}}} = Re_g^{-0.38} Re_f^{0.16} C_w^{-0.13} \quad (5)$$

In which, C_w , defined by Ishii and Grolmes [20], is used to account for the effect of the surface tension on the circulation/dissipation flow in the wave. The wave velocity has an increasing trend of wave celerity for the increase of both gas and liquid superficial velocities, and vice-versa. When the gas core flows over the leeward face of the disturbance wave (volume one), the momentum variation from volume one gives,

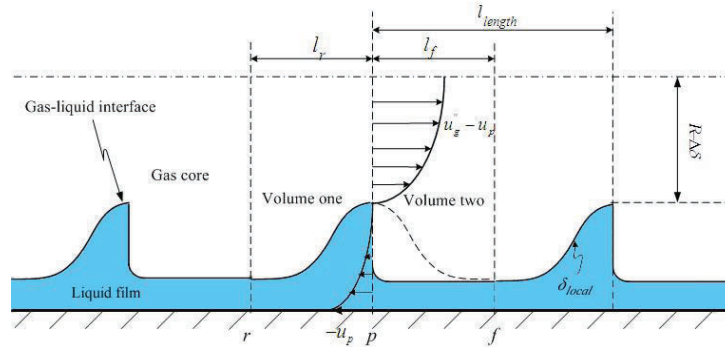


Fig. 3. Schematic of the physical model in the moving frame with speed u_p

$$\Delta M_r = -\rho_g g \pi \int_0^{l_r} (R - \delta_{local})^2 dl + (A_r P|_r - A_p P|_p) - 2\pi \int_0^{l_r} \tau_{i,r} (R - \delta_{local}) dl \quad (6)$$

The terms on the right hand side of Eq. 6 represent the gravity, pressure difference and interfacial shear stress from left to right respectively. In view of the momentum loss of the gas core due to the entrainment-deposition process and formation of gas eddy caused by the sharp extension of cross-section [12], the momentum reduction from volume two is different from the momentum gain from volume one. As for the volume two, obviously, the momentum gain from volume one is identical to the momentum reduction from volume two if ignoring the influence of the entrainment, deposition and eddy on pressure losses. Because the gas core velocity profile at the rear and front of the disturbance wave are the same by ignoring the gas expansion effect due to the axial pressure drop. In contrast, provided that gas eddy and entrainment-deposition effect exist in volume two, the momentum gain from volume one is not equal to the momentum reduction from volume two. In view of this, supposed that part of the momentum gained from volume one, $\lambda \Delta M_r$, investing in the momentum loss due to the entrainment-deposition process and formation of gas eddy results in,

$$-\Delta M_f = (1 - \lambda) \Delta M_r \quad (7)$$

Where, λ denotes the ratio of momentum loss caused by the entrainment-deposition process and formation of gas eddy to the momentum gained from volume one. Therefore, the momentum reduction from volume two can be expressed,

$$-(1 - \lambda) \Delta M_r = -\rho_g g \pi \int_0^{l_f} (R - \delta_{local})^2 dl - (A_f P|_f - A_p P|_p) - 2\pi \int_0^{l_f} \tau_{i,f} (R - \delta_{local}) dl \quad (8)$$

In pursuit of the influence of entrainment-deposition process and formation of gas eddy on the interfacial shear stress, many references [5, 10, 11] have devoted the researches to this matter so far. Thereby, the entrainment-deposition process and formation of gas eddy can be implemented directly here.

$$\lambda \Delta M_r = \frac{-2\pi \int_0^{l_f} R_D U_D (R - \delta_{local}) dl + 2\pi \int_0^{l_f} R_E U_E (R - \delta_{local}) dl}{\pi \int_0^{l_f} \Delta P_e [R^2 - (R - \delta_{local})^2] dl} \quad (9)$$

Where, R_E and R_D are the entrainment rate and the deposition rate respectively which can be obtained from Ishii and Kataoka [15, 21].

$$R_E = R_D = 0.022 \rho_f j_f Re_f^{-0.26} \left(\frac{\mu_g}{\mu_f} \right)^{0.26} E^{0.74} \quad (10)$$

At steady state conditions, the rates of deposition and entrainment are equal, resulting in an equilibrium entrainment fraction of droplets, E , in the gas core. U_E is the mean axial velocity of entraining drops taken as the wave velocity and U_D is the mean axial velocity of depositing drops which is taken as 80% the mean gas velocity based upon Fore and Dukler [22]. δ_{local} is the local liquid film thickness.

For the gas phase flows of interest, as shown in the Fig. 1, when the gas core goes through the disturbance wave, it will encounter a sudden flow cross-sectional area expansion which will result in rolling eddy [23]. Pressure loss caused by gas eddy in the volume two is evaluated as follow based upon Cao [24]

$$\Delta P_e = \frac{K \rho_g^*}{2} (u_g - u_{yf})^2 \quad (11)$$

Where, K is the coefficient representative of pressure loss due to the sudden flow cross-sectional area expansion which is assumed to be 0.3 based upon Zapke et al. [25]. Summing up Eq. 6 and Eq. 7 results in,

$$\begin{aligned} \lambda \Delta M_r = & -[\rho_g^* g \pi \int_0^{l_r} (R - \delta_{local})^2 dl + \rho_g^* g \pi \int_0^{l_f} (R - \delta_{local})^2 dl] \\ & + (A_r P|_r - A_f P|_f) - 2\pi \int_0^{l_{length}} \tau_i (R - \delta_{mean}) dl \end{aligned} \quad (12)$$

Where, l_{length} is the disturbance wave length, which is defined as,

$$l_{length} = l_f + l_r \quad (13)$$

and to make this model tractable, the interfacial shear stress gives,

$$\int_0^{l_{length}} \tau_i (R - \delta_{mean}) dl \cong \int_0^{l_f} \tau_{i,f} (R - \delta_{local}) dl + \int_0^{l_r} \tau_{i,r} (R - \delta_{local}) dl \quad (14)$$

In pursuit of the leeward and upwind face length (l_r and l_f), unfortunately, it is not straightforward to find reliable data in the open literature for describing the parameters largely because most experiments have been designed to study other features of annular flow. Hall Taylor et al. [17] displays a new model for the disturbance wave that the disturbance wave is partitioned into two regions, i.e. an isolated regions of unknown constant vorticity liquid, behind which the gas separates to produces a recirculating wake, which also has constant vorticity. In implementing that model, an assumption that the two regions are symmetrical in shape has been proposed. Therefore, based upon the assumption proposed by Hall Taylor et al. [17] and to make the analysis more tractable herein, l_f is assumed equal to l_r .

3.2. Performance of Model

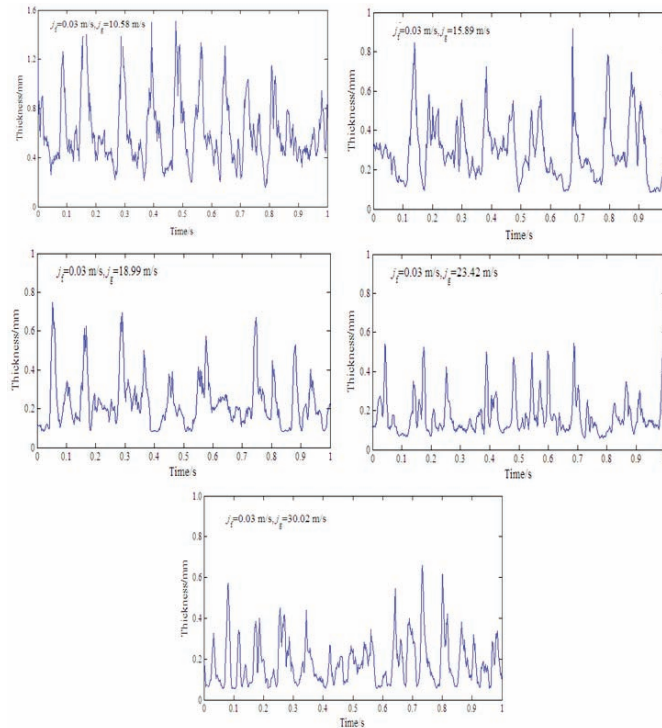


Fig. 4. Liquid film thickness time trace ($j_l \approx 0.03$ m/s)

Solutions of those integral equations need the local disturbance wave profiles, i.e. local wave shapes, δ_{local} , and wave spacing. The liquid film thickness time trace ($j_f \approx 0.03$ m/s) by mean of the Matlab code analysis of the high-speed video images of vertical upflow has attained as shown in Fig. 4. The detailed descriptions of high-speed imaging system and the image processing method can be found in our previous work [26].

However, this method is restricted to extract the spatial variation of the liquid film thickness because of the limited size of images (13 mm totally in axial direction). Therefore, a similar method as used by Hall Taylor et al. [17] has been applied to reproduce the liquid film thickness time trace as a spatial profile in Fig. 5, assuming a steady travelling wave velocity, u_p , to convert the time domain to the space domain.

From the point of view of the modeling, the paramount ingredients of the disturbance waves are uniform wave spacing (wave length) and identical local wave shapes. However, as can be seen from the Fig. 5, although the liquid film typically consists of wavy part and base or substrate, the local wave shapes and spaces between disturbance waves are anomalous which is hard to be implemented in the modeling. In view of this, some assumptions are indispensable for this matter, i.e. uniform wave spacing and disturbance wave height. The wave spacing equals to the total length of the film thickness time trace divided by the number of peaks that appear in the entire time trace. In an effort to generate information specifically and exclusively on the number of peaks, an in-house, dedicated MATLAB script is developed to count peaks with large amplitudes (defined in this work as having amplitudes 1.6 times the mean film thickness or more) according to Zhao et al. [27].

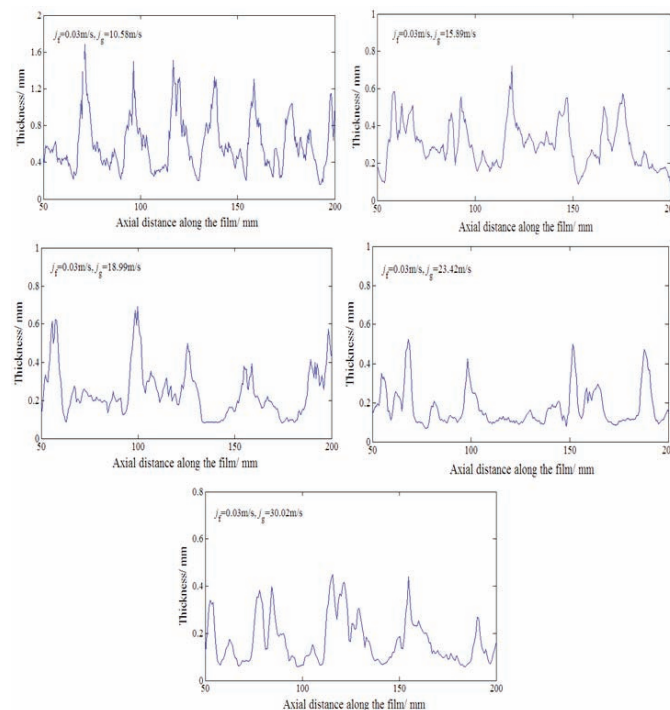


Fig. 5. Spatial wave profile inferred from liquid film thickness time trace

With reference to the local wave shapes, generally, the slope of the leeward face changes more abruptly than that of the upwind face (seldom exceeds 5%) [23] and it should be noted that the axes in Fig. 5 is not to scale which indicates that the disturbance wave is chartered by extremely small aspect ratio. Although the Fig. 5 demonstrates the spatial profile of the local disturbance waves, there still exists an intractable problem, i.e. solutions of those integral equations being restricted to the anomalous shapes from the perspective of the modeling. In view of this, an executable local wave shape in the model should be proposed. Holowach et al. [18] proposed a wave shape in terms of sine wave to predict the droplet entrainment in heated annular flow. However, it is very complicated when his model being applied to calculate the surface tension force for the geometry of the deforming wave. Given that the interfacial shear stress is predominantly affected by the disturbance wave height (disturbance wave being recognized as a source of entrainment-deposition and eddy) rather than by the detailed wave shapes. Thereby, the local wave shapes can be reproduced approximately by mean of the method applied to the paper of Hall Taylor et al. [17], i.e. the local disturbance wave is partitioned into two symmetrical regions starting with the identified local wave peak, and the local wave shapes can be attained by extending forward and backward respectively for the length of half wave spacing [14] as shown in Fig. 6.

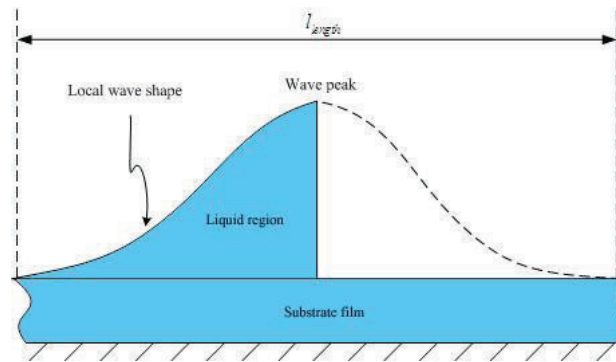


Fig. 6. Schematic of the local wave shape

Fig. 7 shows the detailed local wave profiles which is on the basis of the wave shape and disturbance wave data attained from the Matlab code analysis of the high-speed video images.

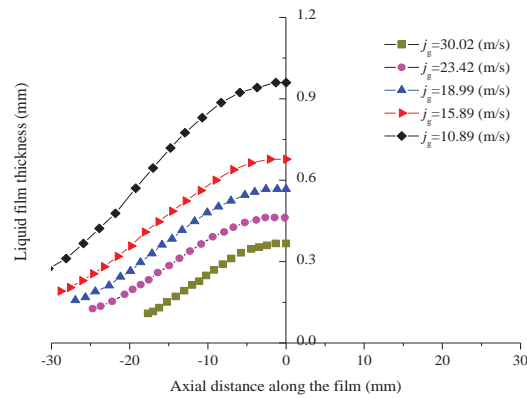


Fig. 7. Local disturbance wave shapes

3.3. Interfacial Shear Stress

For the cases found in annular two-phase flow, the interfacial shear stress generally shows an increasing trend with the increase of both gas and liquid superficial velocities, and vice-versa. A similar tendency acquired by mean of the current model is depicted in Fig. 8, which is consistent with the results of Alamu [9]. As gas superficial velocity increases at fixed liquid superficial velocity, the slip within the gas-liquid interface increases, leading to a higher interfacial shear, and hence the pressure-gradient increases as illustrated in Fig. 2.

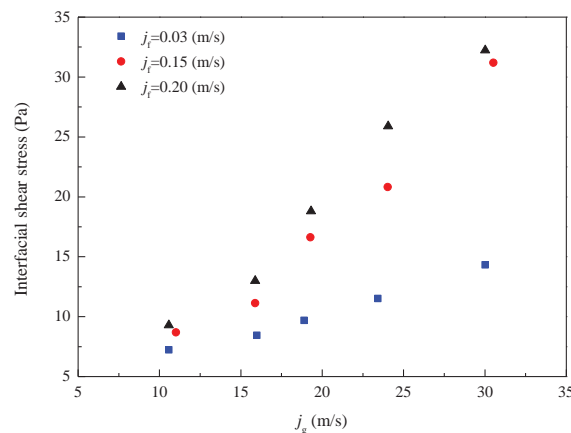


Fig. 8. Interfacial shear stress variation with gas superficial velocity

The results to be shown in the Fig. 8 indicate that the interfacial shear stress is closely linked to both gas and liquid velocity, and the viscosity is crucial for the interfacial shear stress as demonstrated by Fukano [28]. Therefore, the interfacial shear stress can be expressed as the function of gas, liquid velocity and viscosity. Given that the Reynolds number is the ratio of inertia force to the viscosity force, thereby, the interfacial shear stress can be processed in the forms of Reynolds number. In view of this, the interfacial shear stress should be in the dimensionless form. Rearranging Eq. 12 by mean of dividing by $2\pi R l_{length} \rho_g j_g^2$ yields,

$$c_{fw} = c_{fi} - c_{fs} \quad (15)$$

Where, the c_{fw} represents the non-dimensional pressure drop due to the entrainment-deposition and eddy, and the additional gravity pressure drop caused by the variation of density in the gas core, i.e.,

$$c_{fw} = \frac{\lambda \Delta M_r}{2\pi R l_{length} \rho_g j_g^2} + \frac{R(\rho_g - \rho_l)g}{2 l_{length} \rho_g j_g^2} \int_0^{l_{length}} \left(1 - \frac{\delta_{local}}{R}\right)^2 dl \quad (16)$$

c_{fs} denotes the non-dimensional pressure drop originating from the interfacial shear stress,

$$c_{fs} = \frac{1}{\rho_g j_g^2} \left[\frac{1}{l_{length}} \int_0^{l_{length}} \tau_i \left(1 - \frac{\delta_{mean}}{R}\right) dl \right] \cong \frac{\tau_i}{\rho_g j_g^2} \quad (17)$$

c_{fi} being the non-dimensional measured pressure drop given by.

$$c_{fi} = \frac{(A_r P|_r - A_f P|_f) - \rho_g g \pi \int_0^{l_{length}} \left(1 - \delta_{local}\right)^2 dl}{2\pi R l_{length} \rho_g j_g^2} \quad (18)$$

On basis of the MLR (Multiple Linear Regression) processing of c_{fs} in the forms of liquid and gas Reynolds number respectively by using current experimental data gives,

$$c_{fs} = 33.6 \text{Re}_g^{-0.91} \text{Re}_f^{0.30} \quad (19)$$

To validate the availability of the above correlation, Schubring's data [29], which are available in literature, are used to verify. It should be noted here that Schubring's data [29] were obtained under the condition of liquid superficial velocities ranging from 0.03 m/s~ 0.35 m/s for vertical upward annular flow having a diameter of 2.24 cm, and superficial gas velocities envelope of 10 m/s~ 85 m/s at atmospheric pressure. As depicted in Fig. 9, the present correlation can satisfactorily predict not only the current experimental interfacial shear stress, but also the Schubring's data under different work conditions with the maximum relative error of $\pm 25\%$, which indicates that the current model is capable of predicting the interfacial shear stress. It should be emphasized here that the Schubring's data were calculated based upon three different models, i.e. Wallis [3], Fore et al. [5], Hurlburt et al. [30].

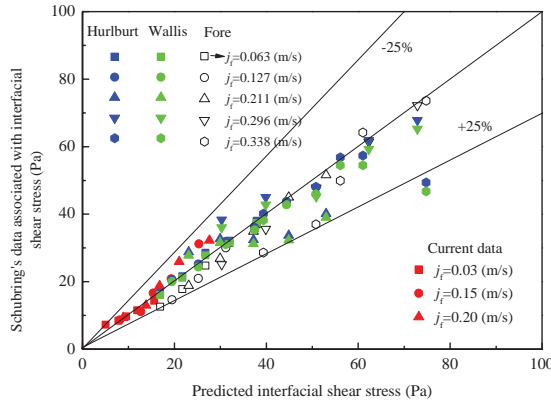


Fig. 9. Comparison of interfacial shear stress vs. liquid superficial velocity predicted by present correlation with current experimental data (D=2.54 cm) and Schubring's data (D=2.24 cm).

4. CONCLUSIONS

Air-water vertical upward annular flow experiments have been conducted at different gas and liquid velocity conditions in a tubular test section having an inside diameter 2.54 cm to obtain the pressure gradients that can provide data to implement a prediction model of gas-liquid interfacial shear stress for vertical annular flow. The model takes the gas-liquid interfacial characteristics (including local wave shapes, disturbance wave spacing, and mobility of the interface) and entrainment-deposition process and gas eddy effect into account. The results of the current model show that the interfacial shear stress has an increasing trend for the increase of both gas and liquid superficial velocities, and the non-dimensional pressure drop originating from the interfacial shear stress, c_{fs} , is in the form of $c_{fs} = 33.6 \text{Re}_g^{-0.91} \text{Re}_f^{0.30}$.

NOMENCLATURE

A	cross-sectional area of gas core, m^2
c_{fs}	non-dimensional pressure drop originating from the interfacial shear stress
c_{fi}	non-dimensional measured pressure gradient
c_{fv}	non-dimensional pressure drop defined in Eq. (13)
D	tube diameter, m
f_i	interfacial shear factor
g	gravitational acceleration, m/s^2
j	superficial velocity, m/s
l_{length}	disturbance wave length, m
ΔM	momentum difference in gas core, N
P	pressure, Pa
ΔP_e	pressure drop caused by gas eddy, Pa
R	tube radius, m
R_D	droplet deposition rate
R_E	entrainment rate
Re	Reynolds number
u_g	gas core velocity, m/s
u_{if}	liquid film velocity, m/s
u_p	disturbance wave propagation velocity, m/s
U_D	mean axial velocity of depositing drops, m/s
U_E	mean axial velocity of entraining drops, m/s

Greek symbols

δ_{local}	local liquid film thickness, m
λ	fraction of momentum gain investing in the momentum loss due to the entrainment-deposition process and formation of gas eddy
ρ	density, kg/m^3
τ_i	interfacial shear stress, Pa

Subscripts

f	front of disturbance wave, liquid phase
g	gas core
i	interfacial
p	disturbance wave peak
r	rear of disturbance wave

ACKNOWLEDGMENTS

The authors are grateful for the support of the Natural Science Foundation of China (Grant No: 51376201), and the authors also want to appreciate the helps provided by Mr. Xiaohong Yang and Mr. Qinzhi Zhu from School of Nuclear Engineering, Purdue University.

REFERENCES

1. B.J. Azzopardi, Disturbance wave frequencies, velocities and spacing in vertical annular two-phase flow, *Nuclear Engineering and Design*, **92**(2) (1986) 121-133.
2. P. Sawant, M. Ishii, T. Hazuku, T. Takamasa, M. Mori, Properties of disturbance waves in vertical annular two-phase flow, *Nuclear Engineering and Design*, **238**(12) (2008) 3528-3541.
3. G.B. Wallis, One Dimensional Two-Phase Flow, McGraw-Hill, New York, 1969.
4. [4] J.C.B. Lopes, Dukler, A.E., Droplet entrainment in vertical annular flow and its contribution to momentum transfer, *AIChE J*, **32** (1986) 1500-1515.
5. L.B. Fore, S.G. Beus, R.C. Bauer, Interfacial friction in gas-liquid annular flow: Analogies to full and transition roughness, *International Journal of Multiphase Flow*, **26**(11) (2000) 1755-1769.
6. R. Kumar, D.P. Edwards, Interfacial shear modelling in two-phase annular flow, in: Proceedings of the 1996 ASME *International Mechanical Engineering Congress and Exposition*, pp. 381-389.
7. R.V.A. Oliemans, B.F.M. Pots, N. Trompé, Modelling of annular dispersed two-phase flow in vertical pipes, *International Journal of Multiphase Flow*, **12**(5) (1986) 711-732.

8. I.N. Alves, E.F. Caetano, K. Minami, O. Shoham, Modeling annular flow behavior for gas wells, *SPE Production Engineering*, **6**(4) (1991) 435-440.
9. M.B. Alamu, Investigation of Periodic Structures in Gas-Liquid Flow, Nottingham, 2010.
10. L.B. Fore, A.E. Dukler, Droplet deposition and momentum transfer in annular flow, *AIChE J*, **41**(9) (1995) 2040-2046.
11. R.J. Belt, J.M.C. Van't Westende, L.M. Portela, Prediction of the interfacial shear-stress in vertical annular flow, *International Journal of Multiphase Flow*, **35**(7) (2009) 689-697.
12. D.M. Maron, N. Brauner, Role of interfacial mobility in determining the interfacial shear factor in two-phase wavy film flow, *International Communications in Heat and Mass Transfer*, **14**(1) (1987) 45-55.
13. J.C. Asali, G.W. Leman, T.J. Hanratty, Entrainment measurements and their use in design equations, PCH, *Physico Chemical Hydrodynamics*, **6**(1-2) (1984) 207-221.
14. Zhaolin Wang, D.L.M. Kamiel S. Gabriel *, The influences of wave height on the interfacial friction in annular gas-liquid flow under normal and microgravity conditions, *International Journal of Multiphase Flow*, **30** (2004) 1193-1211.
15. M. Ishii, K. Mishima, Droplet entrainment correlation in annular two-phase flow, *International Journal of Heat and Mass Transfer*, **32**(10) (1989) 1835-1846.
16. H. Han, A Study of Entrainment in Two-Phase Upward Cocurrent Annular Flow in a Vertical Tube, University of Saskatchewan, 2005.
17. N.S. Hall Taylor, I.J. Hewitt, J.R. Ockendon, T.P. Witelski, A new model for disturbance waves, *International Journal of Multiphase Flow*, **66**(0) (2014) 38-45.
18. M.J. Holowach, L.E. Hochreiter, F.B. Cheung, A model for droplet entrainment in heated annular flow, *International Journal of Heat and Fluid Flow*, **23**(6) (2002) 807-822.
19. C. Berna, A. Escrivá, J.L. Muñoz-Cobo, L.E. Herranz, Review of droplet entrainment in annular flow: Interfacial waves and onset of entrainment, *Progress in Nuclear Energy*, **74**(0) (2014) 14-43.
20. M. Ishii, M.A. Grolmes, Inception criteria for droplet entrainment in two-phase concurrent film flow, *AIChE J*, **21**(2) (1975) 308-318.
21. I. Kataoka, M. Ishii, A. Nakayama, Entrainment and desposition rates of droplets in annular two-phase flow, *International Journal of Heat and Mass Transfer*, **43**(9) (2000) 1573-1589.
22. L.B. Fore, A.E. Dukler, Distribution of drop size and velocity in gas-liquid annular flow, *International Journal of Multiphase Flow*, **21**(2) (1995) 137-149.
23. D.M. Maron, N. Brauner, The role of interfacial mobility in determining the interfacial shear factor in two-phase wavy film flow, *International Communications in Heat and Mass Transfer*, **14**(1) (1987) 45-55.
24. X. Cao, Effect of rolling condition on two-phase flow pattern in vertical tubes, Harbin Engineering University, 2006.
25. A. Zapke, D.G. Kröger, Countercurrent gas-liquid flow in inclined and vertical ducts — I: Flow patterns, pressure drop characteristics and flooding, *International Journal of Multiphase Flow*, **26**(9) (2000) 1439-1455.
26. Liangming Pan, Hui He, Peng Ju, Takashi Hibiki, Mamoru Ishii, Experimental study and modeling of disturbance wave height of vertical annular flow, *International Journal of Heat and Mass Transfer*, **89** (2015) 165-175.
27. Y. Zhao, C.N. Markides, O.K. Matar, G.F. Hewitt, Disturbance wave development in two-phase gas-liquid upwards vertical annular flow, *International Journal of Multiphase Flow*, **55**(0) (2013) 111-129.
28. T. Fukano, T. Furukawa, Prediction of the effects of liquid viscosity on interfacial shear stress and frictional pressure drop in vertical upward gas-liquid annular flow, *International Journal of Multiphase Flow*, **24**(4) (1998) 587-603.
29. D. Schuring, Behavior Interrelationships in Annular Flow, University of Wisconsin-Madison, 2008.
30. E.T. Hurlburt, L.B. Fore, R.C. Bauer, A two zone interfacial shear stress and liquid film velocity model for vertical annular two-phase flow, in: 2006 2nd ASME *Joint U.S.-European Fluids Engineering Summer Meeting*, 2006.